REPORT

Return to Mercury: A Global Perspective on MESSENGER's First Mercury Flyby

Sean C. Solomon,[1]* Ralph L. McNutt Jr.,[2] Thomas R. Watters,[3] David J. Lawrence,[2] William C. Feldman,[4] James W. Head,[5] Stamatios M. Krimigis,[2,6] Scott L. Murchie,[2] Roger J. Phillips,[7] James A. Slavin,[8] Maria T. Zuber[9]

In January 2008, the MErcury Surface, Space ENvironment, GEochemistry, and Ranging (MESSENGER) spacecraft became the first probe to fly past the planet Mercury in 33 years. The encounter revealed that Mercury is a dynamic system; its liquid iron-rich outer core is coupled through a dominantly dipolar magnetic field to the surface, exosphere, and magnetosphere, all of which interact with the solar wind. MESSENGER images confirm that lobate scarps are the dominant tectonic landform and record global contraction associated with cooling of the planet. The history of contraction can be related to the history of volcanism and cratering, and the total contractional strain is at least one-third greater than inferred from Mariner 10 images. On the basis of measurements of thermal neutrons made during the flyby, the average abundance of iron in Mercury's surface material is less than 6% by weight.

Mercury, the closest planet to the Sun, is the smallest of the inner planets of our solar system and in many ways the most unusual (*1*). Its high bulk density implies that an iron-rich core makes up 60% or more of its mass (*2*), a fraction at least twice that of any other planet. Mercury's heavily cratered surface points to early cessation of internal geological activity (*3*), yet its outer core is molten (*4*), and it is the only inner planet other than Earth to have an internal magnetic field (*5*). The first spacecraft to visit Mercury was Mariner 10, which flew by three times in 1974 and 1975 and imaged about 45% of the planet's surface (*6*). In January 2008, the MErcury Surface, Space ENvironment, GEochemistry, and Ranging (MESSENGER) spacecraft (*7*) became only the second probe to encounter the planet en route to its insertion into orbit about Mercury in March 2011. The broad range of observations made during MESSENGER's first flyby illuminate the strongly dynamic interactions among Mercury's interior, surface, tenuous atmosphere, and magnetosphere.

The January flyby was the first of three, each to be followed by a propulsive maneuver near the next aphelion, needed to reduce the arrival speed at Mercury to the point that orbit insertion can be accomplished (*8*). The Mercury flybys and subsequent maneuvers yield successive orbits having ratios of the orbital period of Mercury to that of the spacecraft of about 2:3, 3:4, and 5:6. In January, the spacecraft approached Mercury from the night side and crossed the dawn terminator shortly after closest approach at an altitude of 201 km (Fig. 1). MESSENGER viewed the sunlit side of Mercury, including about 21% of the planet's surface never imaged by Mariner 10, primarily on departure. Observations totaling about 500 MB in volume were acquired by all MESSENGER instruments, including 1213 images obtained by the Mercury Dual Imaging System (MDIS) (*9*).

Mercury's iron-rich core is central to the dynamical interactions that govern the planet's geology, exosphere, and magnetosphere. The planet's magnetic field is the result of a magnetic dynamo in the molten outer core, although whether that dynamo is currently operating (*10*–*12*) or operated only in the past and imparted a long-wavelength remanent or frozen field to Mercury's outer crust (*13*) has been a matter of debate. MESSENGER confirmed that Mercury's internal field is dominantly dipolar and indicated that there may be a quadrupole component, but no shorter-wavelength crustal anomalies were detected near closest approach (*14*). The last two results are not supportive of an entirely remanent field (*13*) and therefore point to a modern dynamo, but the contribution of crustal fields cannot be fully assessed until low-altitude measurements are made over more of the surface. Because maintenance of a dynamo requires an energy source such as freezing of an inner core or precipitation of solid iron from an outer core containing lighter elements alloyed with iron (*15*), the history of Mercury's magnetic field is closely tied to the core's thermal history and bulk composition. That core thermal history is likely expressed in the deformation of Mercury's surface.

For the 45% of Mercury's surface viewed by Mariner 10, the dominant deformational structures are lobate scarps, interpreted on the basis of morphology and the deformation of earlier impact features to be the surface expression of thrust faults formed by horizontal shortening of the crust (*16*). Lobate scarps cut across all major geological units and display a broad distribution of orientations. These characteristics led to the hypothesis that lobate scarps formed during an episode of global contraction that followed the end of heavy-impact bombardment of the inner solar system (*16*). The cumulative amount of contractional strain accommodated by the lobate scarps mapped from Mariner 10 images, inferred from topographic relief (*16*) and dimensional scaling relations (*17*), is 0.05 to 0.1%. When extrapolated to the entire planetary surface, this total strain provides an important constraint on models for the thermal history of Mercury's core and mantle (*18*). A number of questions were raised by the Mariner 10 results, however, including whether the 55% of the surface not imaged during that mission would display similarly pervasive contrac-

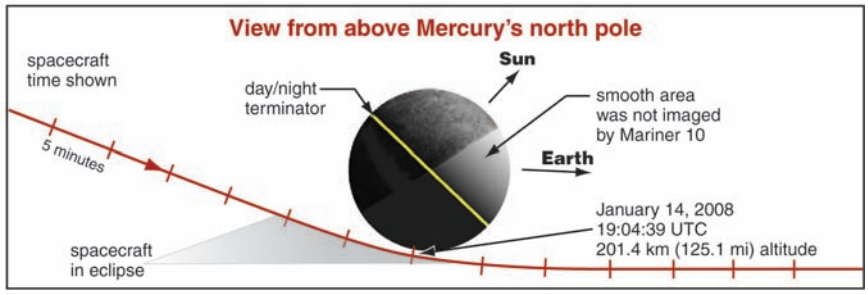

Fig. 1. Trajectory of the first MESSENGER flyby of Mercury viewed in a Mercury-fixed coordinate system from above Mercury's north pole. The spacecraft traveled from left to right. Shown are the time the spacecraft was in eclipse, the position of the terminator during the flyby, the hemisphere of Mercury previously imaged by Mariner 10, and the point of closest approach.

[1]Department of Terrestrial Magnetism, Carnegie Institution of Washington, Washington, DC 20015, USA. [2]Space Department, Johns Hopkins University Applied Physics Laboratory, Laurel, MD 20723, USA. [3]Center for Earth and Planetary Studies, National Air and Space Museum, Smithsonian Institution, Washington, DC 20560, USA. [4]Planetary Science Institute, Tucson, AZ 85719, USA. [5]Department of Geological Sciences, Brown University, Providence, RI 02912, USA. [6]Academy of Athens, Athens 11527, Greece. [7]Southwest Research Institute, Boulder, CO 80302, USA. [8]NASA Goddard Space Flight Center, Greenbelt, MD 20771, USA. [9]Department of Earth, Atmospheric, and Planetary Sciences, Massachusetts Institute of Technology, Cambridge, MA 02139, USA.

*To whom correspondence should be addressed. E-mail: scs@dtm.ciw.edu

tional faults, whether the identified scarps provide a reliable means for estimating the total contraction since the era of heavy bombardment, and whether limits could be placed on when the contraction occurred relative to other geological events preserved at Mercury's surface.

MESSENGER images of an additional 21% of Mercury's surface not previously viewed by spacecraft show that contractional fault structures are widespread and diverse in geometry. As in the area imaged by Mariner 10, lobate scarps are the most prominent tectonic landform. Such scarps range to 600 km in length (Fig. 2). Other contractional features, including wrinkle ridges and high-relief ridges, are also evident. The only areas imaged by either Mariner 10 or MESSENGER within which extensional, rather than contractional, faults have been documented are the interior of the 1550-km-diameter Caloris basin (*19*) and a small portion of the inner floor of the younger 250-km-diameter Raditladi peak-ring basin (*20*); for both features, the extensional faults are probably the result of postimpact uplift of the basin floor (*16*, *19*). MESSENGER images provide numerous examples of craters that have been substantially deformed and shortened by younger lobate scarps (Fig. 3), confirming that the scarps are contractional and providing additional opportunities to infer the magnitude of horizontal shortening accommodated in such areas. In the examples of Fig. 3, the horizontal displacement on the faults beneath each of the lobate scarps must have been at least one to several kilometers to account for the distortions of the older craters they have cut.

MESSENGER obtained images of many areas viewed by Mariner 10 but at different resolution and, at least as importantly, at different lighting conditions. Many tectonic features not recognized from Mariner 10 images can be identified in MESSENGER images of those same areas (Fig. 4). These newly recognized features indicate that the average contractional strain of Mercury's surface recorded by lobate scarps exceeds the estimates obtained from Mariner 10 observations alone. The summed length of lobate scarps in the portion of the surface imaged by both Mariner 10 and MESSENGER, together with a displacement-length scaling relation for faults on Mercury (*17*), yields an average contraction one-third greater than previous estimates. Moreover, the average contraction estimated from the total length of scarps recognized in regions newly imaged by MESSENGER is comparable to this larger figure. Because neither MESSENGER nor Mariner 10 images were obtained at optimum lighting conditions for the recognition of low-relief tectonic features in all areas, this new estimate is a minimum.

Most models of the cooling of Mercury's mantle and core (*18*) have predicted that the accumulated contractional strain since the end of heavy bombardment ~3.8 billion years ago was greater than the strain estimated from the geometry of lobate scarps identified in Mariner 10 images (*17*). The models most consistent with the Mariner 10 results had a comparatively creep-resistant (anhydrous) mantle, slowly decaying interior heat production (dominated by ^{232}Th as opposed to the shorter-lived ^{235}U and ^{40}K), and a large amount (>6% by weight) of a lighter element such as S in Mercury's outer core to retard the growth of a solid inner core (*18*). An increase by at least one-

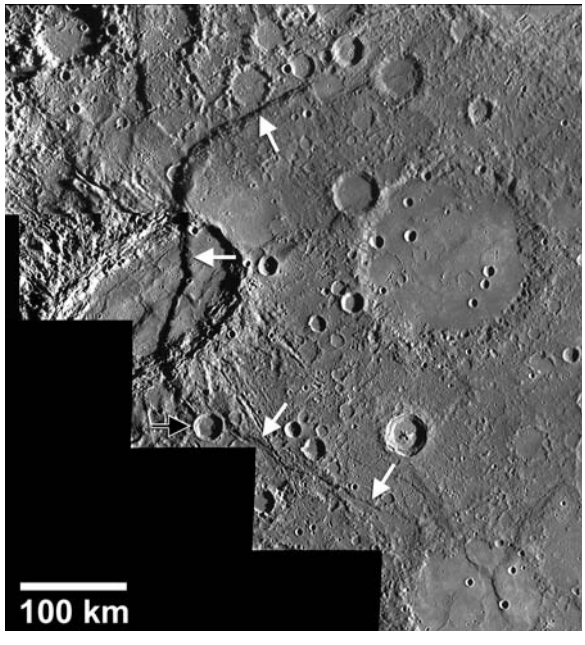

Fig. 2. Beagle Rupes, a prominent lobate scarp (white arrows) imaged on the portion of Mercury's surface viewed for the first time by MESSENGER, is more than 600 km long and offsets the floor and walls of the ~220-km-diameter, elliptically shaped impact crater Sveinsdóttir. The floor of the impact crater was flooded by smooth plains and subsequently deformed by wrinkle ridges before scarp development. Beagle Rupes is one of the most arcuate of the lobate scarps found on Mercury to date. A ~30-km-diameter crater sits undeformed on the northwest-southeast segment of Beagle Rupes (black arrow). This MDIS monochrome (750-nm) narrow-angle camera (NAC) image mosaic is centered at about 3°S, 103.5°E; north is to the top in this and other images and mosaics. The relative positions on the planet of the area in this image, other images in this paper, and images and profiles in companion papers are depicted in fig. S1. The mosaic consists of NAC frames EN0108825899M, EN0108825904M, EN0108826004M, EN0108826095M, EN0108826100M, EN0108826105M, EN0108826191M, EN0108826196M, EN0108826201M, EN0108826206M, EN0108827037M, and EN0108827042M.

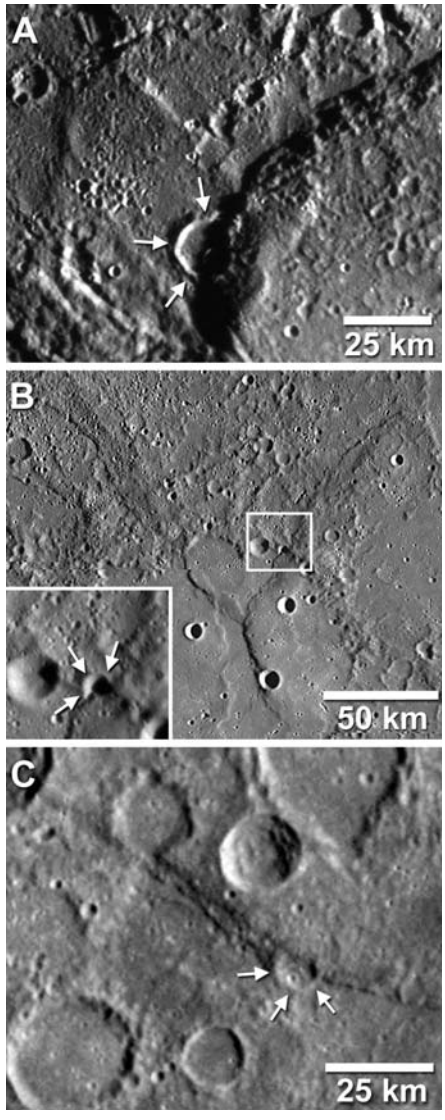

Fig. 3. Three examples of craters substantially deformed by a lobate scarp. In each case, portions of the crater floor and rim have been buried by overthrusted material. (**A**) The northern segment of Beagle Rupes has crosscut a ~17-km-diameter impact crater (centered near 0.3°N, 101°E; arrows) on intercrater plains. From NAC frame EN0108827037M. (**B**) The northeast-southwest–trending segment of a lobate scarp has cut a ~5-km-diameter impact crater (centered near 7.9°S, 108.2°E; see inset) located near the rim of a larger degraded impact crater that was flooded by smooth plains and subsequently deformed by wrinkle ridges. This mosaic consists of NAC frames EN0108825899M, EN0108825904M, EN0108825994M, and EN0108825999M. (**C**) A northwest-southeast–trending lobate scarp has deformed an ~11-km-diameter crater (centered near 16.5°S, 133°E) on intercrater plains. From NAC frame EN0108828317M.

third in the average preserved contractional strain will relax one or more of these model restrictions and permit a greater range of possible planetary thermal histories.

Additional information on the timing of global contraction relative to other major events in Mercury's geological evolution can be derived from MESSENGER observations. From Mariner 10 images it was seen that scarps deform all major geological units, including the comparatively young smooth plains, but no instance of a scarp embayed by plains was recognized (*16*). A candidate for such an embayment relation was imaged by MESSENGER (Fig. 5). This and similar relations, together with the abundance of evidence that smooth plains are volcanic deposits (*19*, *21*), indicate that scarp development began before many smooth plains were emplaced and continued after the eruption of the youngest appreciable expanse of smooth plains material yet observed. Whereas a number of lobate scarps deformed older craters (Figs. 2 to 4), there are also many examples of undeformed craters superposed on scarps (e.g., Figs. 2 and 5). These relations offer the promise that the rate of global contraction subsequent to late heavy bombardment can be estimated and tied to the history of plains emplacement. Such records would constrain the evolution of mantle temperatures and the rate of growth of the solid inner core and its potential as a power source for Mercury's core dynamo.

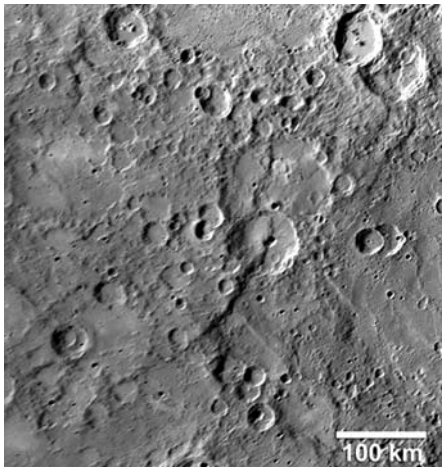

Fig. 4. This ~270-km-long lobate scarp, which deformed the two large craters in the center of the mosaic, was not visible in Mariner 10 images of the area, because during the Mariner 10 flybys the Sun was locally at a high angle to the surface. This mosaic is centered near 24°S, 254°E, and uses images acquired before the flyby closest approach. The mosaic consists of NAC frames EN0108821370M, EN0108821375M, EN0108821397M, and EN0108821402M.

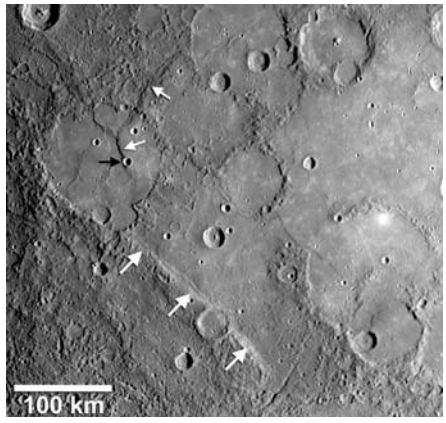

Fig. 5. Possible embayment of lobate scarps by smooth plains. Smooth plains material, interpreted to consist of volcanic flows, appears to have ponded against the structural relief of a preexisting lobate scarp formed in older intercrater plains (lower set of thick white arrows). Low-relief ridges in the smooth plains just outward of the scarp face may be evidence of continued movement on the underlying thrust fault after plains emplacement. In the upper left (upper set of thin white arrows), a lobate scarp cuts across both intercrater plains (topmost arrow) and smooth plains that filled the floor of a ~120-km-diameter impact crater (Fig. 3B). Slip on the fault scarp appears to postdate the formation of wrinkle ridges formed in the smooth plains interior to the crater. Shown also is the undeformed crater superposed on this scarp (black arrow). This mosaic is centered near 10°S, 110°E, and uses images acquired on departure from closest approach. The mosaic consists of NAC frames EN0108828307M, EN0108828312M, EN0108828359M, and EN0108828364M.

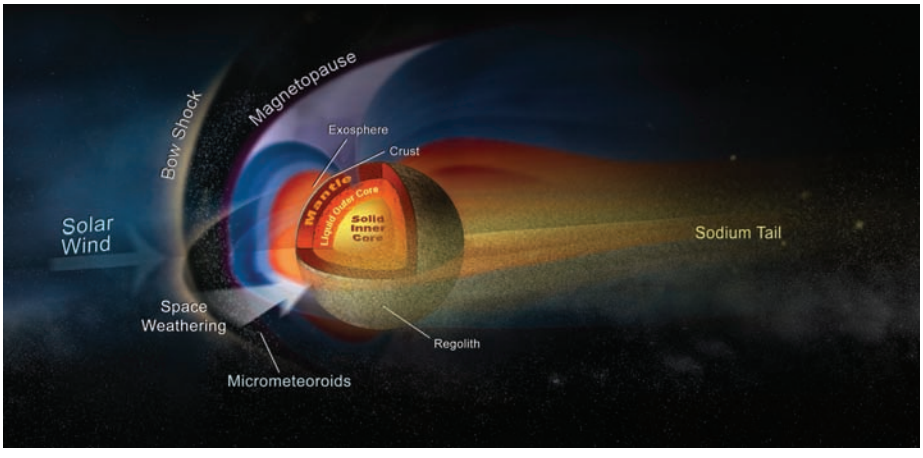

Fig. 6. Schematic depiction of several of the interconnections among Mercury's interior, surface, exosphere, magnetosphere, and interplanetary environment.

Even though Mercury is more than 60% Fe by weight, the average Fe abundance of Mercury's surface materials, and by inference its crust and mantle, is lower than those of the other inner planets (*22*). This contrast is rooted in planetary formational processes (*1*), but distinguishing among competing hypotheses requires accurate measurements of the structure (*23*) and major-element chemistry (*24*) of Mercury's crust. MESSENGER detected no absorption features attributable to Fe^{2+} in silicates either in disk-averaged or higher–spatial resolution visible and near-infrared spectra (*25*) or with multispectral imaging (*26*). The generally red spectral slopes displayed by Mercury surface materials (*25*, *26*) have been attributed to nanometer-scale particles of Fe metal, originating from meteoritic iron or reduction of iron-bearing surface minerals and redeposited from vapor by space weathering processes accompanying meteoroid and charged-particle impacts (*27*). The most direct information on surface Fe abundance must await measurements by the Gamma-Ray and Neutron Spectrometer (GRNS) (*28*) once MESSENGER is in orbit about Mercury.

An upper limit on surface Fe abundance can be estimated from measurements made by the Neutron Spectrometer (NS) sensor on GRNS. Thermal neutrons provide information about surface abundances of neutron-absorbing elements, e.g., Fe, Ti, Gd, and Sm (*29*). MESSENGER's NS can measure thermal neutrons with Doppler filter spectroscopy (DFS) (*30*), which uses the spacecraft speed (~7 km/s) to separate slowly moving thermal neutrons (~2 km/s) from more energetic epithermal neutrons. DFS was applied to the flyby observations and made use of a 90° spacecraft rotation near closest approach to provide separate measurements of Doppler shifted (J_+) and nonshifted (J_0) neutrons. The ratio $J_0/(J_+ - J_0)$ provides an estimate of the thermal neutrons from Mercury, which can then be related to the abundances of neutron-absorbing elements. Lunar soils provide approximate analogs to Mercury surface materials because of their low H content and their wide ranges of Fe and Ti abundances. On the basis of a comparison of Mercury flyby measurements with modeled neutron fluxes for a range of lunar soils (*31*), the upper-limit neutron absorption content is less than that of the comparatively low-Fe Luna 20 soil, for which neutron absorption is nonetheless dominated by Fe, at 5.8% by weight (*32*). If all neutron absorption in Mercury's soil were due to Fe, then the MESSENGER data suggest that the

Fe abundance is less than ~6% and would be lower still if Ti, Gd, or Sm is present. For comparison, the average Fe abundance is about 5% and 8% in Earth's continental and oceanic crust, respectively, and 5% in lunar highlands crust (*33*).

During its flyby, MESSENGER provided a comprehensive view of solar wind interaction with Mercury's magnetic field and neutral atmosphere and, indirectly, its surface. At the time of the flyby, solar activity was low and, in contrast with Mariner 10 observations, no energetic charged particles with energies above ~30 keV were detected (*34*). Magnetometer observations (*14*) of the magnetospheric boundaries, current systems, and plasma waves confirm that this magnetosphere appears structurally to be a miniature of that of Earth. One notable difference is the presence of a double current sheet at the dawn terminator that likely represents heavy planetary ion effects unique to Mercury (*34*). The Mercury Atmospheric and Surface Composition Spectrometer observed neutral Na and Ca in Mercury's exosphere—delivered from surface materials in part by the same micrometeoroid and ion-impact processes that space-weather the surface—and mapped the structure of Mercury's antisunward Na tail (*35*). The Fast Imaging Plasma Spectrometer sensor on the Energetic Particle and Plasma Spectrometer instrument (*36*) observed a range of heavy magnetospheric plasma ions—including O^+, Na^+, Mg^+, K^+, Ca^+, S^+, and H_2S^+—derived from the exosphere or surface (*37*). On the basis of the full set of observations made during MESSENGER's first flyby, Mercury is seen to be a dynamic planet where the interactions among core, surface, exosphere, magnetosphere, and interplanetary environment are strongly interlinked (Fig. 6). Subsequent encounters under different solar conditions and one Earth year in orbit about Mercury as the Sun approaches the next maximum in the solar cycle should permit MESSENGER to explore these interactions across their full range of behavior.

References and Notes

1. S. C. Solomon, *Earth Planet. Sci. Lett.* **216**, 441 (2003).
2. H. Harder, G. Schubert, *Icarus* **151**, 118 (2001).
3. P. D. Spudis, J. E. Guest, in *Mercury*, F. Vilas, C. R. Chapman, M. S. Matthews, Eds. (Univ. of Arizona Press, Tucson, 1988), pp. 118–164.
4. J. L. Margot, S. J. Peale, R. F. Jurgens, M. A. Slade, I. V. Holin, *Science* **316**, 710 (2007).
5. N. F. Ness, K. W. Behannon, R. P. Lepping, Y. C. Whang, *J. Geophys. Res.* **80**, 2708 (1975).
6. B. C. Murray, *J. Geophys. Res.* **80**, 2342 (1975).
7. S. C. Solomon, R. L. McNutt Jr., R. E. Gold, D. L. Domingue, *Space Sci. Rev.* **131**, 3 (2007).
8. J. V. McAdams, R. W. Farquhar, A. H. Taylor, B. G. Williams, *Space Sci. Rev.* **131**, 219 (2007).
9. S. E. Hawkins III *et al.*, *Space Sci. Rev.* **131**, 247 (2007).
10. S. Stanley, J. Bloxham, W. E. Hutchison, M. T. Zuber, *Earth Planet. Sci. Lett.* **234**, 27 (2005).
11. M. H. Heimpel, J. M. Aurnou, F. M. Al-Shamali, N. Gomez Perez, *Earth Planet. Sci. Lett.* **236**, 542 (2005).
12. U. R. Christensen, *Nature* **444**, 1056 (2006).
13. O. Aharonson, M. T. Zuber, S. C. Solomon, *Earth Planet. Sci. Lett.* **218**, 261 (2004).
14. B. J. Anderson *et al.*, *Science* **321**, 82 (2008).
15. B. Chen, J. Li, S. A. Hauck II, *Geophys. Res. Lett.* **35**, L07201, 10.1029/2008GL033311 (2008).
16. R. G. Strom, N. J. Trask, J. E. Guest, *J. Geophys. Res.* **80**, 2478 (1975).
17. T. R. Watters, M. S. Robinson, A. C. Cook, *Geology* **26**, 991 (1998).
18. S. A. Hauck II, A. J. Dombard, R. J. Phillips, S. C. Solomon, *Earth Planet. Sci. Lett.* **222**, 713 (2004).
19. S. L. Murchie *et al.*, *Science* **321**, 73 (2008).
20. R. G. Strom, C. R. Chapman, W. J. Merline, S. C. Solomon, J. W. Head III, *Science* **321**, 79 (2008).
21. J. W. Head *et al.*, *Science* **321**, 69 (2008).
22. M. S. Robinson, G. J. Taylor, *Meteorit. Planet. Sci.* **36**, 841 (2001).
23. M. T. Zuber *et al.*, *Science* **321**, 77 (2008).
24. W. V. Boynton *et al.*, *Space Sci. Rev.* **131**, 85 (2007).
25. W. E. McClintock *et al.*, *Science* **321**, 62 (2008).
26. M. S. Robinson *et al.*, *Science* **321**, 66 (2008).
27. B. Hapke, *J. Geophys. Res.* **106**, 10039 (2001).
28. J. O. Goldsten *et al.*, *Space Sci. Rev.* **131**, 339 (2007).
29. W. C. Feldman *et al.*, *J. Geophys. Res.* **105**, 20347 (2000).
30. W. C. Feldman, D. M. Drake, *Nucl. Instrum. Methods Phys. Res. A* **245**, 182 (1986).
31. D. J. Lawrence *et al.*, *J. Geophys. Res.* **111**, E08001, 10.1029/2005JE002637 (2006).
32. L. Haskin, P. Warren, in *Lunar Sourcebook*, G. Heiken, D. Vaniman, B. M. French, Eds. (Cambridge Univ. Press, New York, 1991), pp. 357–474.
33. K. Lodders, B. Fegley Jr., *The Planetary Scientist's Companion* (Oxford Univ. Press, New York, 1998), pp. 140 and 177.
34. J. A. Slavin *et al.*, *Science* **321**, 85 (2008).
35. W. E. McClintock *et al.*, *Science* **321**, 92 (2008).
36. G. B. Andrews *et al.*, *Space Sci. Rev.* **131**, 523 (2007).
37. T. H. Zurbuchen *et al.*, *Science* **321**, 90 (2008).

38. The hundreds of engineers and technical support personnel who brought MESSENGER from a concept to a successful flight project warrant the sustained appreciation of the mission science team. We also thank L. M. Prockter for assembling fig. S1. The MESSENGER project is supported by the NASA Discovery Program under contracts NASW-00002 to the Carnegie Institution of Washington and NAS5-97271 to Johns Hopkins University Applied Physics Laboratory.

Supporting Online Material

www.sciencemag.org/cgi/content/full/321/5885/59/DC1
Fig. S1
References

28 April 2008; accepted 3 June 2008
10.1126/science.1159706

REPORT

Spectroscopic Observations of Mercury's Surface Reflectance During MESSENGER's First Mercury Flyby

William E. McClintock,[1]* Noam R. Izenberg,[2] Gregory M. Holsclaw,[1] David T. Blewett,[2] Deborah L. Domingue,[2] James W. Head III,[3] Jörn Helbert,[4] Timothy J. McCoy,[5] Scott L. Murchie,[2] Mark S. Robinson,[6] Sean C. Solomon,[7] Ann L. Sprague,[8] Faith Vilas[9]

During MESSENGER's first flyby of Mercury, the Mercury Atmospheric and Surface Composition Spectrometer made simultaneous mid-ultraviolet to near-infrared (wavelengths of 200 to 1300 nanometers) reflectance observations of the surface. An ultraviolet absorption (<280 nanometers) suggests that the ferrous oxide (Fe^{2+}) content of silicates in average surface material is low (less than 2 to 3 weight percent). This result is supported by the lack of a detectable 1-micrometer Fe^{2+} absorption band in high-spatial-resolution spectra of mature surface materials as well as immature crater ejecta, which suggests that the ferrous iron content may be low both on the surface and at depth. Differences in absorption features and slope among the spectra are evidence for variations in composition and regolith maturation of Mercury's surface.

Before MESSENGER's first flyby of Mercury on 14 January 2008, our knowledge of the planet's surface mineralogy came from low-spatial-resolution, ground-based spectroscopic observations. Early disk-integrated observations showed a low-albedo, relatively featureless spectrum that increases monotonically across the visible to near-infrared wavelengths, a characteristic referred to as a "red" spectral slope (*1*–*3*). On the Moon these spectral characteristics result from space weathering, a process in which amorphous silica coatings containing nanometer-scale metallic iron (nanophase metallic iron, $npFe^0$) darken exposed regolith, increase spectral slope, and reduce spectral contrast (*4*, *5*). Although Mercury's surface appears to be highly space-weathered, the absence of identifiable near-infrared absorptions argues for a low average ferrous iron content (*2*, *6*, *7*). This view is supported by recent mid-infrared emission spectra and reflectance observations that have been interpreted to indicate the presence of plagioclase feldspar and low-iron orthopyroxene (enstatite) (*6*, *8*, *9*) and high-Ca clinopyroxene (*10*). These mid-infrared spectra support the presence of Na-bearing feldspar and Mg-rich minerals (*8*), which are present in very-low-iron terrestrial rock types. To more fully understand Mercury's surface composition, it is necessary to explore regional spectral variations across units that contain relatively unweathered materials, such as ejecta from small craters, which are often less than 100 km